Uptake of positron emission tomography tracers in experimental bacterial infections: a comparative biodistribution study of radiolabeled FDG, thymidine, L-methionine, ^{67}Ga-citrate, and ^{125}I-HSA

Yoshifumi Sugawara[1], Tomasz D. Gutowski[1], Susan J. Fisher[1], Raya S. Brown[1], Richard L. Wahl[1,2]

[1] Division of Nuclear Medicine, Department of Internal Medicine, The University of Michigan Medical Center, Ann Arbor, Michigan, USA
[2] Department of Radiology, The University of Michigan Medical Center, Ann Arbor, Michigan, USA

Received 26 September and in revised form 18 December 1998

Abstract. The purpose of this study was to evaluate the localization of positron emission tomography (PET) tracers [2-deoxy-2-fluoro-D-glucose (FDG), thymidine, and L-methionine] in sites of bacterial infection, and to contrast this with that of other tracers. The left calf muscles of rats were infected with a suspension of *Escherichia coli* and the biodistribution of ^{18}F- or ^{3}H-FDG, ^{3}H-thymidine, L-^{11}C- or ^{3}H-methionine, gallium-67 citrate (^{67}Ga-citrate) and iodine-125 human serum albumin (^{125}I-HSA) was determined in these animals. ^{3}H-FDG uptake in the infectious foci was evaluated by autoradiography of histological sections. Although ^{18}F-FDG, ^{67}Ga-citrate, and ^{125}I-HSA showed comparatively high uptake in the infected muscle [the percentage activity of injected dose (ID) per gram of tissue normalized for rat weight in kilogram (%ID/g)×kg at 2 h postinjection was as follows: ^{18}F-FDG, 0.184±0.026 to 0.218±0.046; ^{67}Ga-citrate, 0.221±0.016; ^{125}I-HSA, 0.198±0.019], the infected muscle to blood ratio was much higher for ^{18}F-FDG than for ^{67}Ga-citrate or ^{125}I-HSA (^{18}F-FDG, 10.31±0.76 to 14.89±2.26; ^{67}Ga-citrate, 1.24±0.67; ^{125}I-HSA, 0.20±0.02). The draining reactive lymph nodes also showed higher accumulation of ^{18}F-FDG than of ^{67}Ga-citrate or ^{125}I-HSA. The uptake of ^{3}H-thymidine and L-^{11}C- or ^{3}H-methionine in the infected muscle was lower than that of ^{18}F- or ^{3}H-FDG (at 2 h postinjection, ^{3}H-thymidine = 0.039±0.005 and L-^{3}H-methionine = 0.063±0.007 (%ID/g)×kg. Autoradiographs showed that the highest ^{3}H-FDG uptake was seen in the area of inflammatory cell infiltration surrounding the necrotic region. In conclusion, ^{18}F-FDG, which rapidly accumulates in sites of bacterial infection and in reactive lymph nodes with a high target to background ratio, appears to be a promising infection detection agent.

Correspondence to: R.L. Wahl, Division of Nuclear Medicine, University of Michigan Medical Center, 1500E Medical Center Drive, B1G505C, Ann Arbor, MI 48109-0028, USA

Key words: Bacterial infection – Fluorodeoxyglucose – Thymidine – L-Methionine – Gallium-67 citrate

Eur J Nucl Med (1999) 26:333–341

Introduction

Increased rates of glucose metabolism [1], amino acid transport [2], and DNA synthesis [3] are often present in tumors. For these reasons, successful tumor imaging has been possible with positron emission tomography (PET) imaging, using positron-emitter labeled analogs of glucose, amino acids, and DNA precursors [4–6]. 2-deoxyglucose traces aspects of glucose metabolism [4], L-methionine reflects amino acid transport and protein synthesis [7, 8], and thymidine traces cell proliferation [9]. However, much less is known regarding the uptake of these tracers in infections, although it has been reported that [^{18}F]-2-deoxy-2-fluoro-D-glucose (^{18}F-FDG) shows substantial uptake in some human and experimental infections [10–15].

In clinical practice, gallium-67 citrate (^{67}Ga-citrate) has been used widely for evaluation of infectious lesions [16]. However, there are several disadvantages in using a standard gamma camera with ^{67}Ga-citrate as a tracer. Suitable images can be obtained only after some delay, usually 24–72 h after injection, and the sensitivity, resolution, and ability to assess abdominal lesions are low due to the substantial background uptake [16]. If ^{18}F-FDG accumulates rapidly in infections, it may represent a preferred infection detection agent [17–19]. Further, understanding the uptake of thymidine and L-methionine in infections is of practical importance, as it has been suggested that these agents have lower uptake into infections than does ^{18}F-FDG [13].

To evaluate the feasibility of using PET tracers to detect bacterial infections, we (a) compared the accumulation of ^{18}F-FDG into *Escherichia coli* (*E. coli*)-induced

muscle infections in rodents with that of ^{67}Ga-citrate and iodine-125 human serum albumin (^{125}I-HSA); (b) compared the uptake and biodistribution of [methyl-^{3}H]thymidine (^{3}H-Thy) and L-[methyl-^{11}C]methionine (^{11}C-Met) or L-[methyl-^{3}H]methionine (^{3}H-Met) with that of ^{18}F-FDG or [5,6-^{3}H]-2-fluoro-2-deoxy-D-glucose (^{3}H-FDG) in the same rodent infection models; and (c) investigated the precise location of ^{3}H-FDG uptake in the site of infection by autoradiography of histological sections of the infected muscle.

Materials and methods

Rodent infection models. A suspension of *E. coli* (isolated from human infections) was prepared in sterile saline (2×10^{9} organisms/ml) according to the McFarland turbidity standard [20, 21] (which is commonly used in the clinical microbiology laboratory) by spectrophotometry (wavelength 670 nm, absorbance 0.680, DU-64 Spectrophotometer, Beckman Instruments Inc., Fullerton, Calif.). *E. coli* is a well-studied free-living bacterial organism and a frequent cause of bacterial infections in humans [22]. Groups of healthy female Sprague Dawley rats (total, $n = 56$) were inoculated in the left calf muscles with 0.1–0.2 ml of the suspension of *E. coli* ($n = 50$) or 0.1 ml of sterile saline (for controls, $n = 6$), and when swelling was apparent (2–4 days later), they were used for the study. The animals were maintained on a regular rodent chow diet, but were fasted overnight (with water accessible) before tracer injections. All animal experiments were conducted with the approval of the Unit of Laboratory Animal Medicine, a certified animal care organization, following the "Principles of laboratory animal care" (NIH publication No. 86-23, revised 1985).

Radiopharmaceuticals. ^{18}F-FDG was produced by nucleophilic fluorination [23], ^{11}C-Met was synthesized by methylation of homocysteine with ^{11}C-methyl iodide [24], and ^{125}I-HSA was radiolabeled by the iodogen method [25]. ^{67}Ga-citrate was purchased commercially from DuPont Merck Radiopharmaceuticals (North Billerica, Mass.). ^{3}H-Thy, ^{3}H-Met, and ^{3}H-FDG were obtained from American Radiolabeled Chemicals Inc. (St. Louis, Mo.).

Five types of paired radiolabeled tracers (^{18}F-FDG/^{125}I-HSA, ^{18}F-FDG/^{67}Ga-citrate, ^{18}F-FDG/^{3}H-Thy, ^{18}F-FDG/^{3}H-Met, and ^{3}H-FDG/^{11}C-Met) were prepared. The volume of tracer solutions in sterile saline ranged from 0.2 to 0.3 ml and doses were approximately as follows: ^{18}F-FDG = 1.85–5.55 MBq (50–150 µCi), ^{125}I-HSA = 1.85 MBq (50 µCi), ^{67}Ga-citrate = 1.85 MBq (50 µCi), ^{3}H-Thy = 1.48 MBq (40 µCi), ^{3}H-Met = 9.25 MBq (250 µCi), ^{3}H-FDG = 1.85 MBq (50 µCi), ^{11}C-Met = 7.40 MBq (200 µCi).

Biodistribution studies. The solutions of paired radiolabeled tracers were injected intravenously. The rats (total, $n = 56$) were sacrificed at several intervals from injection time. Ten rats (six for the saline control study, four for the *E. coli* study) were sacrificed at 2 h after ^{18}F-FDG/^{125}I-HSA injections, 15 rats (five at 30 min, five at 2 h and five at 6 h) after ^{18}F-FDG/^{67}Ga-citrate injections, 16 rats (four at 20 min, five at 1 h and seven at 2 h) after ^{18}F-FDG/^{3}H-Thy injections, and 15 rats (five at 20 min, four at 1 h and six at 2 h) after ^{18}F-FDG/^{3}H-Met or ^{3}H-FDG/^{11}C-Met injections. Tissues were excised and weighed, and the tracer activity in tissues determined with a gamma counter or liquid scintillation counter. Although ^{18}F and ^{11}C radioactivity levels were counted immediately after the tissue excision, ^{125}I and ^{67}Ga radioactivity levels were counted at least 24 h following sacrifice, to eliminate any contribution from high-energy ^{18}F activity [26]. ^{3}H radioactivity levels were measured by beta counting in a 1600 TR Packard liquid scintillation analyzer (Meriden, Conn.) at least 2 days after sacrifice. After appropriate decay correction for each tracer, the percentage activity of injected dose (ID) per gram of tissue, normalized for rat weight in kilograms (%ID/g)×kg, was determined and compared [27].

Autoradiography. Sets of three consecutive 16-µm-thick frozen sections of infected left calf muscles and of the normal right calf muscles from two additional rats were sectioned at intervals of about 800 µm, collected on frozen slides (–20°C) and quickly dried on a hot plate to minimize diffusion. The dried sections and a set of calibrated plastic standards (12 plastic standards with 1000-fold range of ^{14}C concentrations for which the relationship between the exposure produced by ^{3}H in tissue and that produced by the ^{14}C plastic standards is known [28]) were placed in X-ray cassettes and apposed to hyperfilm-[^{3}H] (Amersham, Arlington Heights, Ill.) at 4°C for 34 days [29]. The films were developed in Kodak D-19 developer, full strength, for 4 min, dipped in 1% acetic acid and fixed in Kodak rapid fixer.

Histology. The histological structures in each set of sections were identified from the first section on each of the autoradiographed slides that was stained with hematoxylin and eosin (H&E) at the end of the exposure period. Distribution of *E. coli* in the infected muscle was evaluated in an additional section that was stained with the BBL Gram Stain kit (Becton Dickinson, Cockeysville, Md.). Quality control slide for gram-positive bacteria and a section of the normal right calf muscle were used as controls for this staining.

Densitometry. Differences in relative ^{3}H-FDG uptake in the abscess and surrounding muscle tissue were estimated from the variations in the relative optical densities of the autoradiographic film images. Each area was examined microscopically and categorized by its predominant histological characteristic as either necrosis (N), inflammatory cell infiltration (I), or damaged muscle (M). The borders of each area were traced on the computerized images of the H&E sections and then superimposed on the matching computerized autoradiographic images. The numerical estimates of activity in chosen areas were measured by means of a computer-assisted video densitometry system (MCID system, Imaging Research Inc. St. Catherine's, Ontario) [28]. The relative densities were expressed as the average apparent disintegrations per minute per microgram (dpm/µg) protein for each area according to the calibrated standards. The values measured from the autoradiographs ranged between 1 and 150 apparent dpm/µg protein and were below the grain density saturation of the film, namely relative densities of 0.106 to 0.570 on a scale of 0–1 (maximum–minimum film transparency). Biases caused by attenuation due to differences in tissue density between different histological categories of the abscess were negligible. The numbers of identifiable macrophages and polymorphonuclear leukocytes were counted in the area of inflammatory cell infiltration around the necrotic region.

Results

Biodistribution studies

^{18}F-FDG vs ^{125}I-HSA. In the saline control group, there was no significant difference in ^{18}F-FDG uptake be-

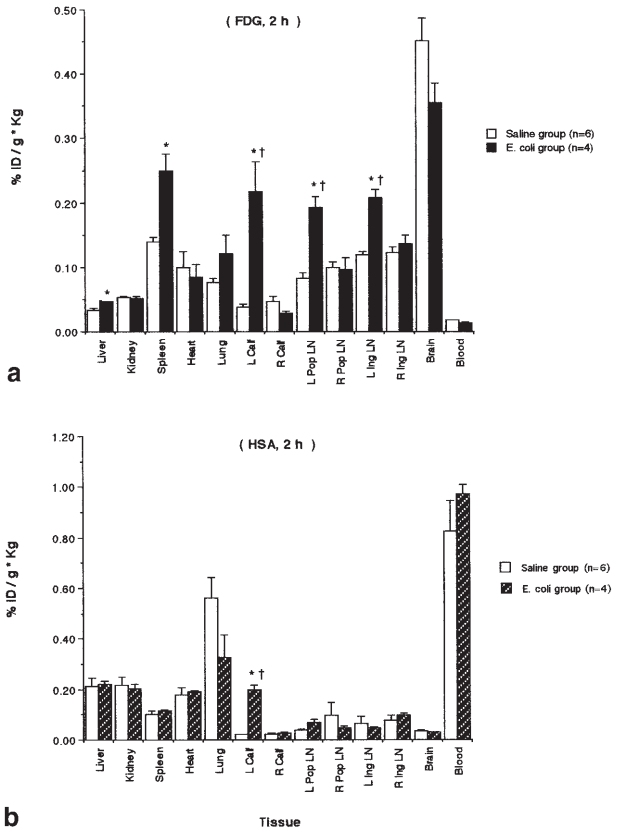

Fig. 1. Tissue biodistribution of ^{18}F-FDG (**a**) and ^{125}I-HSA (**b**) at 2 h post injection in rats. Rats were inoculated in the left calf muscle with saline (saline group, n = 6) or *Escherichia coli* (*E. coli* group, n = 4). Values are mean ± s.e.m. * P<0.05 compared with the saline group; † P<0.05 compared with the right-side tissue. *FDG*, F-2-fluoro-2-deoxy-D-glucose; *HSA*, ^{125}I-human serum albumin; *L*, left; *R*, right; *Pop*, popliteal; *Ing*, inguinal; *LN*, lymph node

tween the saline inoculated side (left) and the contralateral side (Fig. 1a). Similarly, there was no significant difference in ^{125}I-HSA uptake between the inoculated and contralateral sides (Fig. 1b). On the other hand, in the *E. coli*-inoculated group, the ^{18}F-FDG uptake of left calf muscle, left popliteal lymph node, left inguinal lymph node and liver and spleen was significantly increased compared with uptake in the saline control group (P<0.05) (Fig. 1a). ^{18}F-FDG uptake in the infected left calf muscle was 8.45±2.53 times higher than in the right calf muscle, and the uptake of ^{18}F-FDG in the local draining lymph nodes was 2.20±0.45 (popliteal) or 1.58±0.20 (inguinal) times higher than in contralateral lymph nodes (Table 1). Although the ^{125}I-HSA uptake of the left calf muscle was significantly higher (9.9-fold) than that in the saline control group (P<0.05) or that of the right calf muscle (P<0.05), in other tissues, including proximal lymph nodes, there were no significant differences (Fig. 1b). Both ^{18}F-FDG and ^{125}I-HSA showed comparably high uptake in the infected muscle (^{18}F-FDG = 0.218±0.046, ^{125}I-HSA = 0.198±0.019 (% ID/g)×kg; however, the infected muscle to blood ratio was much higher for ^{18}F-FDG than for ^{125}I-HSA (^{18}F-FDG = 14.89±2.26 vs ^{125}I-HSA = 0.20±0.02) (Table 1).

^{18}F-FDG vs ^{67}Ga-citrate. Figure 2 shows the biodistribution and changes over time post injection of ^{18}F-FDG/^{67}Ga-citrate. In the infected left calf muscle, ^{18}F-FDG and ^{67}Ga-citrate showed comparable high uptake (at 2 h following tracer injection: ^{18}F-FDG = 0.216± 0.015, ^{67}Ga-citrate = 0.221±0.016 (%ID/g)×kg (Fig. 2b) and both increased with time; however, the local draining lymph nodes showed higher accumulation of ^{18}F-FDG than of ^{67}Ga-citrate. On the other hand, improved target to background ratios were observed for both ^{18}F-FDG and ^{67}Ga-citrate through 6 h post-injection, but these were much higher for ^{18}F-FDG than for ^{67}Ga-citrate (the infected muscle/blood ratios at 6 h were as follows: ^{18}F-FDG = 18.54±3.41, ^{67}Ga-citrate = 1.07±0.09) (Table 1), since ^{18}F-FDG levels in the blood decreased more rapidly than the levels of ^{67}Ga-citrate.

^{18}F-FDG vs ^{3}H-Thy. Figure 3 shows the biodistribution and changes over time post injection of ^{18}F-FDG/^{3}H-Thy. Although the ^{3}H-Thy uptake in the infected left calf muscle was higher than that in the right calf muscle at 20 min and 1 h post injection, at 2 h post injection it showed no significant difference from that in the right calf muscle. At all time points, the uptake of ^{3}H-Thy in

Table 1. The uptake ratio of the infected side (L) to the noninfected contralateral side (R) or blood for ^{18}F-FDG, ^{125}I-HSA and ^{67}Ga-citrate

Ratio	^{18}F-FDG/^{125}I-HSA study (n = 4)		^{18}F-FDG/^{67}Ga-citrate study (n = 15)					
	^{18}F-FDG	^{125}I-HSA	^{18}F-FDG			^{67}Ga-citrate		
	2 h (n = 4)	2 h (n = 4)	30 min (n = 5)	2 h (n = 5)	6 h (n = 5)	30 min (n = 5)	2 h (n = 5)	6 h (n = 5)
L/R calf M	8.45±2.53	7.97±1.59	7.45±1.10	7.55±1.87	9.69±1.81	3.48±0.63	5.15±0.53	9.81±0.87
L/R Pop LN	2.20±0.45	1.53±0.13	1.58±0.22	1.96±0.14	2.71±0.39	1.17±0.06	1.26±0.08	1.63±0.10
L/R Ing LN	1.58±0.20	0.46±0.07	1.22±0.15	1.78±0.35	1.39±0.15	0.92±0.03	0.93±0.14	1.21±0.05
L calf/blood	14.89±2.26	0.20±0.02	2.04±0.43	10.31±0.76	18.54±3.41	0.39±0.07	1.24±0.67	1.07±0.09

Ratios are represented as the mean ± s.e.m.
L, Left; *R*, right; *M*, muscle; Pop, popliteal; Ing, inguinal; LN, lymph node

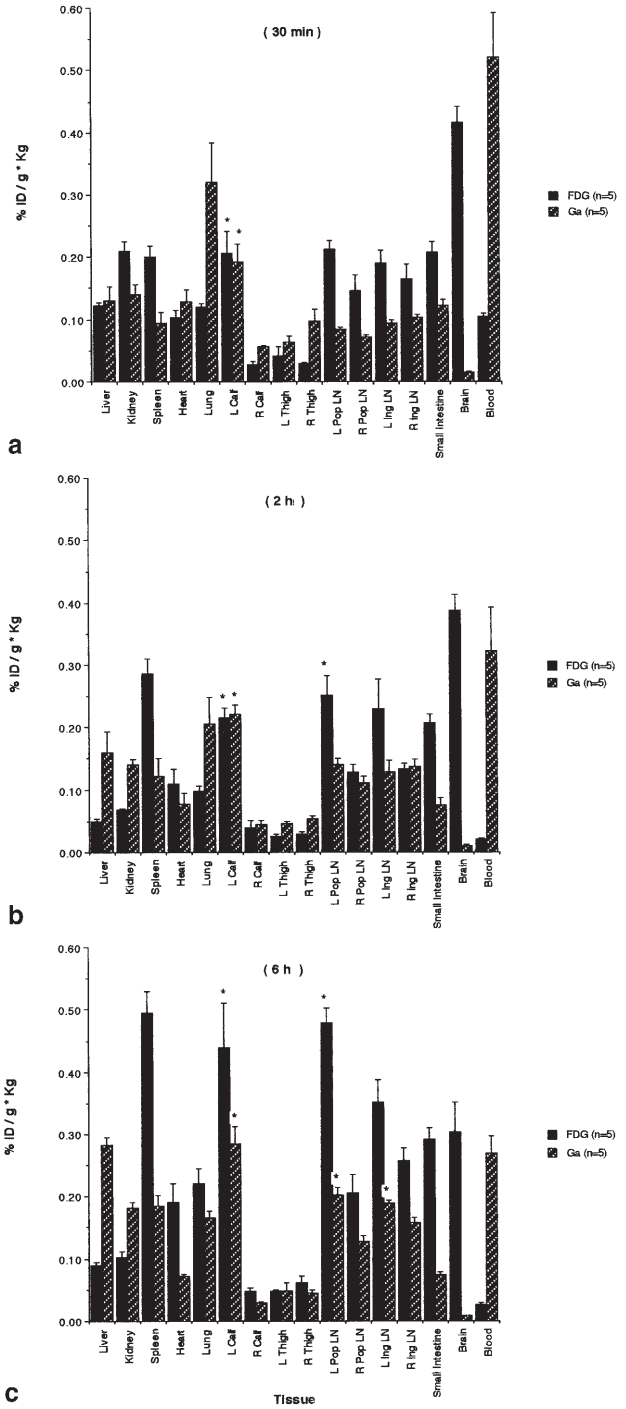

Fig. 2. Tissue biodistribution of ^{18}F-FDG and ^{67}Ga-citrate at 30 min (**a**), 2 h (**b**), and 6 h (**c**) post injection in rats. Rats were inoculated in the left calf muscle with *E. coli*. Values are mean ± s.e.m. * $P<0.05$ compared with the right-side tissue. Ga, ^{67}Ga-citrate; other abbreviations are as in Fig. 1

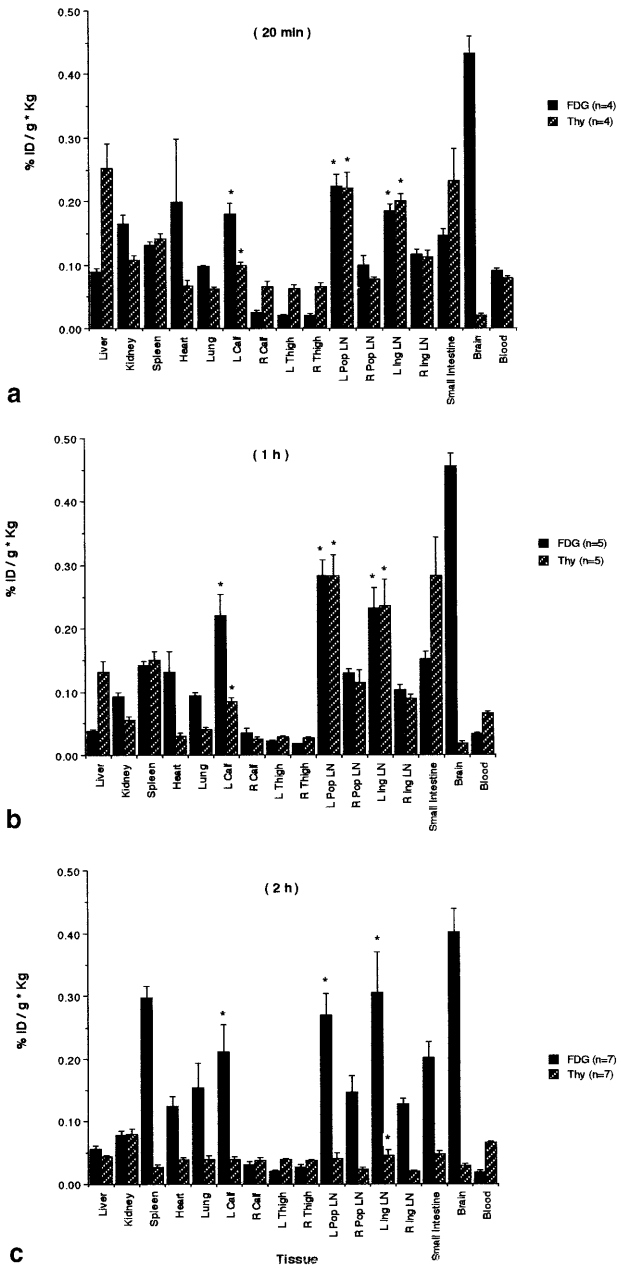

Fig. 3. Tissue biodistribution of ^{18}F-FDG and ^{3}H-Thy at 20 min (**a**), 1 h (**b**), and 2 h (**c**) post injection in rats. Rats were inoculated in the left calf muscle with *E. coli*. Values are mean ± s.e.m. * $P<0.05$ compared with the right-side tissue. *Thy*, ^{3}H-thymidine; other abbreviations are as in Fig. 1

the infected left calf muscle was much lower than that of ^{18}F-FDG. In the local draining lymph nodes, ^{18}F-FDG and ^{3}H-Thy showed comparable high uptake at 20 min and 1 h post injection; however, at 2 h post injection, the uptake of ^{3}H-Thy in these lymph nodes was much lower than that of ^{18}F-FDG. The infected muscle to blood ratios for ^{3}H-Thy were also much lower than those of ^{18}F-FDG through 2 h post injection (the infected muscle/blood ratios at 2 h were as follows: ^{18}F-FDG = 14.46±4.61, ^{3}H-Thy = 0.60±0.08) (Table 2).

^{18}F- or ^{3}H-FDG vs ^{3}H- or ^{11}C-Met. Figure 4 shows the biodistribution and changes over time post injection of ^{3}H-FDG/^{11}C-Met or ^{18}F-FDG/^{3}H-Met. As with ^{3}H-Thy, although increased uptake of ^{3}H- or ^{11}C-Met in the infected left calf muscle and in the local draining lymph nodes was observed to some extent compared with the normal side, these uptake values were lower than those

Table 2. The uptake ratio of the infected side (L) to the noninfected contralateral side (R) or blood for ^{18}F- or ^{3}H-FDG, ^{3}H-Thy and ^{3}H- or ^{11}C-Met

Ratio	^{18}F-FDG/^{3}H-Thy study (n = 16)					^{3}H-FDG/^{11}C-Met study (n = 9)				^{18}F-FDG/^{3}H-Met study (n = 6)	
	^{18}F-FDG			^{3}H-Thy		^{3}H-FDG		^{11}C-Met		^{18}F-FDG	^{3}H-Met
	20 min (n = 4)	1 h (n = 5)	2 h (n = 7)	20 min (n = 4)	1 h (n = 5)	2 h (n = 7)	20 min (n = 5)	1 h (n = 4)	20 min (n = 5)	1 h (n = 4)	2 h (n = 6)	2 h (n = 6)
L/R calf M	7.66±1.25	7.86±2.62	8.36±2.04	1.54±0.11	3.32±0.29	1.15±0.18	5.49±1.25	6.16±1.27	1.39±0.15	2.17±0.28	4.25±0.47	1.31±0.06
L/R Pop LN	2.37±0.38	2.17±0.13	2.08±0.35	2.92±0.45	2.57±0.32	1.78±0.36	2.36±0.46	3.15±0.50	1.82±0.27	1.92±0.22	1.79±0.20	1.44±0.15
L/R Ing LN	1.60±0.09	2.31±0.36	2.38±0.43	1.84±0.23	2.71±0.50	2.17±0.34	1.81±0.34	2.36±0.35	1.46±0.20	1.81±0.16	1.37±0.18	1.25±0.11
L calf / blood	1.99±0.24	6.71±1.18	14.46±4.61	1.27±0.05	1.30±0.17	0.60±0.08	2.14±0.13	3.50±0.64	3.47±0.36	1.96±0.14	14.35±3.45	8.20±3.24

Ratios are represented as the mean ± s.e.m.
Thy, Thymidine; Met, methionine; L, left; R, right; M, muscle; Pop, popliteal; Ing, inguinal; LN, lymph node

Fig. 4. Tissue biodistributions of ^{3}H-FDG and ^{11}C-Met at 20 min (**a**), 1 h (**b**), and ^{18}F-FDG and ^{3}H-Met at 2 hours (**c**) post injection in rats. Rats were inoculated in the left calf muscle with *E. coli*. Values are mean ± s.e.m. * P<0.05 compared with the right-side tissue. *FDG*, ^{3}H- or ^{18}F-2-fluoro-2-deoxy-D-glucose; *Met*, L-^{11}C- or ^{3}H-methionine; other abbreviations are as in Fig. 1

of ^{18}F- or ^{3}H-FDG. The infected muscle/blood ratios for ^{3}H- or ^{11}C-Met were about 50% lower than those for ^{18}F- or ^{3}H-FDG (except at 20 min), while they were clearly higher than those for ^{3}H-Thy (Table 2).

Histology

As a result of the inoculation, an abscess developed near the edge of the left calf muscle (Fig. 5). It consisted of an oval necrotic region (N) that was surrounded by a

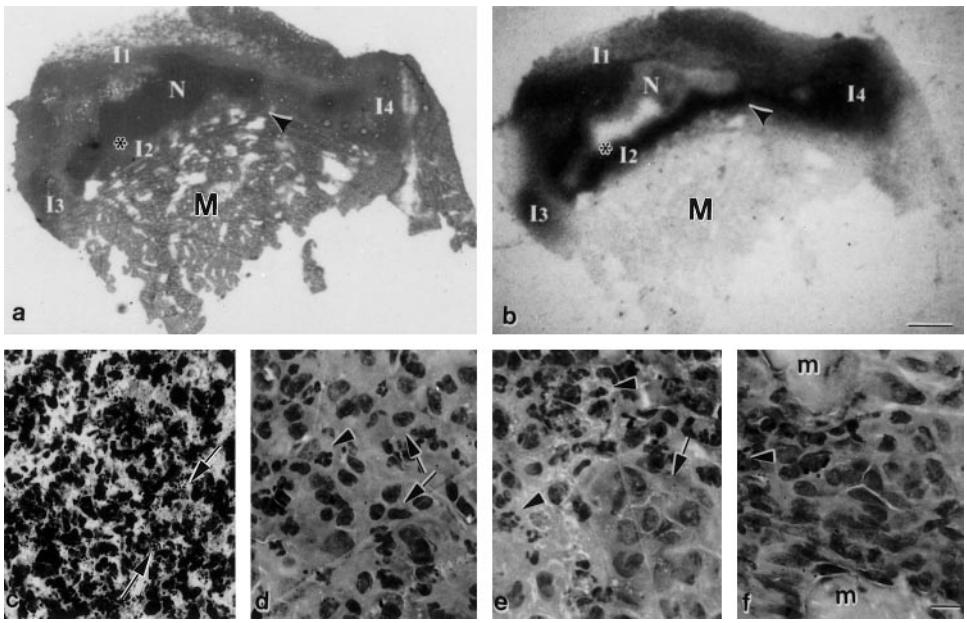

Fig. 5a–f. ^{3}H-FDG uptake in *E. coli*-induced infection. **a,b** A computerized image of a histological section of an infected left calf muscle of rat stained with H&E (**a**) and the corresponding macroautoradiograph (**b**). The central necrotic region (*N*) is surrounded by damaged muscle tissue with heavy inflammatory cell infiltration (I_1–I_4) and edematous muscle (*M*). (×8; bar = 1 mm). **c** Photomicrograph of the necrotic region stained with BBL gram stain. Numerous clusters of bacteria were seen in this area (*arrows*). **d** Photomicrograph from area I_1. **e** Photomicrograph from the necrotic side of area I_2 (* in **a** and **b**). Note the cluster of macrophages (*arrow*). **f** Photomicrograph from the muscle side of area I_2 (*arrowhead* in **a** and **b**). In **d**–**f** *arrowheads* indicate polymorphonuclear cells; *arrows* indicate macrophages; *m*, muscle bundle. (**c**—**f** ×500; bar = 10 µm)

Table 3. ^{3}H-FDG uptake and inflammatory cell count in the infectious foci

	M	N	I_1	I_2	I_3	I_4
^{3}H-FDG uptake (apparent dpm/µg protein) [a]	13±0	45±2	71±0	139±2	118±5	112±2
Inflammatory cell count[b]			102±9	125±10	117±8	80±10
(macrophage count)			(54±7)	(101±10)	(78±5)	(54±5)

Values are mean ± s.e.m.
M, Muscle; N, necrosis; I_1–I_4, areas with heavy inflammatory cell infiltration (Fig. 5)
[a] ^{3}H-FDG uptake was measured in autoradiographs of three consecutive sections of an infected calf muscle
[b] Numbers of inflammatory cells (macrophages + polymorphonuclears) in 400× field (average of five fields/area as seen in Fig. 5)

band comprising infiltrating neutrophils, macrophages (I_1–I_4), and remnants of muscle fibers. On one side of the section, this band was bordered by the edge of the muscle on one side (I_1) and the necrotic area on the other side. In the band on the muscle side (I_2), a gradient in the severity of muscle damage and cell infiltration, from remnants of fibers and many infiltrating cells to undamaged muscle bundles separated by infiltrating cells and interstitial fluids, was observed. The bacteria were mainly concentrated in and around the necrotic area but some clusters could also be seen around the less damaged muscle bundles.

Autoradiography

The autoradiographs showed that ^{3}H-FDG uptake varied in the different regions of the left calf muscle tissue (Fig. 5). No ^{3}H-FDG uptake was detected in the right calf muscle. There was more uptake in areas of inflammatory cell infiltration (I_1–I_4) surrounding the necrosis than in the necrotic region itself or the edematous muscle (Table 3). More ^{3}H-FDG uptake was seen in the areas of heavy inflammatory cell infiltration (Fig. 5). Among the different areas of inflammatory cell infiltration, the highest uptake was in area I_2 which also had the highest counts of infiltrating cells and the highest ratio of macrophages/polymorphonuclear leukocytes (Fig. 5, Table 3).

Discussion

In this study, ^{18}F-FDG was demonstrated to accumulate rapidly in the infectious foci and reactive lymph nodes caused by *E. coli* inoculation, and showed much higher

infection to background ratios at early time points than were obtained for ^{67}Ga-citrate or ^{125}I-HSA. On the other hand, L-^{11}C- or ^{3}H-methionine and particularly ^{3}H-thymidine were less actively accumulated in the infectious foci than ^{18}F- or ^{3}H-FDG. The autoradiographs showed that the highest ^{3}H-FDG uptake was seen in the area of inflammatory cell infiltration surrounding the necrotic region. The infectious foci to blood ratios for ^{18}F-FDG uptake at 2 h post injection found in this study were similar to those reported previously by Wahl et al. [27] for human tumor xenografts to blood ratios (10.31±0.76 to 14.89±2.26 for infection sites vs 12.3±1.8 average for all tumors).

It was first reported by Som et al. [4] that turpentine-induced abscesses in rats showed no ^{18}F-FDG uptake above background, while ^{67}Ga-citrate uptake was high. However, subsequently Tahara et al. [10] reported a case of high ^{18}F-FDG uptake by an abscess in a human in a PET imaging study. Since then, there have been several other reports demonstrating that ^{18}F-FDG may accumulate in a variety of inflammatory lesions [11, 14, 15, 19]. Thus, ^{18}F-FDG may have clinical utility as an infection detection agent.

^{67}Ga-citrate has been widely used clinically for the evaluation of infectious lesions, but generally requires 24–72 h to obtain suitable images. In this study, we found that, compared with ^{67}Ga-citrate, ^{18}F-FDG accumulates more rapidly in infectious foci and reactive lymph nodes and the target to background ratios are much higher (Table 1). While the mechanism of ^{67}Ga-citrate uptake in infections is complex and not yet fully elucidated [16], it is different from that of ^{18}F-FDG uptake. Hoffer [30] has reported high concentrations of lactoferrin in neutrophils and in abscess fluids and suggested that ^{67}Ga-citrate binding to lactoferrin is a major factor in the mechanism of accumulation of ^{67}Ga-citrate in the abscess. On the other hand, ^{18}F-FDG uptake in infectious lesions has been considered due to inflammatory cells (i.e., leukocytes and macrophages) [31–33] and granulation tissue [33, 34]. Activated leukocytes and macrophages in inflammatory tissue utilize glucose as an energy source for chemotaxis and phagocytosis [35] and can increase both oxygen consumption and glucose metabolism in response to infection, via the hexose monophosphate shunt, depending on the cell and the nature of the stimulus [31].

In addition, increased vascular permeability and increased blood flow due to newly formed or dilated blood vessels may cause some increase in local tracer uptake [15, 36]. Indeed, in our study, ^{125}I-HSA uptake was substantially increased (vs normal muscle levels) in the infected left calf muscle (Table 1). However, the contribution of blood activity to the uptake of ^{18}F-FDG in the infectious lesions appeared to be negligible, since the blood activity of ^{18}F-FDG decreases faster and is therefore much lower than that of other tracers.

Besides infectious foci and lymph nodes, liver and spleen also showed higher ^{18}F-FDG uptake in the *E. coli*-infected group than in the saline control group (Fig. 1a). Although we are uncertain of the precise mechanism, it is likely that lymph nodes that filter and "police" the extravascular fluids, and phagocytic cells of the liver and spleen that constitute the "second" line of defense against infection [37], could show high ^{18}F-FDG uptake. Our data show considerably higher ^{18}F-FDG uptake in the spleen, where both phagocytosis and antibody production are increased in response to bacterial infections, than in the liver, where only phagocytosis occurs [38]. The increased uptake of ^{18}F-FDG in the liver and spleen might be a cause of difficulty in the detection of infectious foci in these organs; however further investigations will be required to elucidate this phenomenon.

Recently, Yamada et al. [34] showed high accumulation of ^{18}F-FDG in turpentine-induced inflammatory tissue by means of macro- and micro-autoradiography. However, since in humans, many infections are caused by bacteria or fungi [15] and abscess formation is more common in infections with pyogenic organisms [37], a bacterial infection model, even if it produces somewhat more heterogeneous results, seems to be more physiologically relevant than nonbacterial models, and may be more applicable to clinical conditions.

In the current bacterial model, an abscess was formed and the necrotic area showed slightly higher ^{3}H-FDG uptake than the surrounding edematous muscle (Table 3), while reportedly the center of the abscess in turpentine model showed very low ^{18}F-FDG uptake [34]. This difference could be partly attributed to bacterial ^{3}H-FDG uptake or to the presence of some live infiltrating cells in the necrotic area in our model system. It has been reported that abscess-forming bacteria utilize glucose as an energy source using various pathways [39]. The lack of any ^{18}F-FDG uptake in Som et al.'s report [4] could be attributed to a low numbers of inflammatory cells, lack of granulation tissue, or an absence of microorganisms.

In this study, we also compared the uptake of paired radiolabeled PET tracers (^{18}F-FDG/^{3}H-Thy, ^{18}F-FDG/^{3}H-Met, and ^{3}H-FDG/^{11}C-Met) from 20 min to 2 h after injection, since these short-life PET tracers showed the highest target to blood ratios at these time points in previous tumor studies (^{11}C-Met: 20 min; ^{18}F-FDG: 2 h) [27, 40]. At all time points, substantial ^{18}F- or ^{3}H-FDG uptake was observed in both the infected foci and the reactive lymph nodes, while considerably less ^{3}H-thymidine and L-^{11}C- or ^{3}H-methionine accumulated in the same infectious sites, though they did accumulate to some extent in the lymph nodes. In contrast to nonbacterial models, L-^{11}C- or ^{3}H-methionine showed a reasonably high infection/blood uptake ratio, but the infected muscle/normal muscle uptake ratio was not as high. Indeed, some alteration of protein synthesis and cellular proliferation has been reported in some organs as a result of severe infection or sepsis [41–44]. This alteration might cause an increased background organ uptake of L-^{11}C- or ^{3}H-methionine or ^{3}H-thymidine, and make it difficult to detect infectious foci, even though these tracers

show increased infection/blood uptake ratios. Although the increased blood flow with high vascular permeability and the fibroblast proliferation at the periphery of infections may facilitate the accumulation of L-^{11}C- or ^{3}H-methionine or ^{3}H-thymidine in infectious foci [45], and reactive proliferation of lymph nodes likely increases uptake of both tracers, these tracers do not accumulate in infections to the same extent as does ^{18}F- or ^{3}H-FDG.

In conclusion, ^{18}F- or ^{3}H-FDG rapidly accumulates in bacterial infectious foci and proximal reactive lymph nodes, while L-^{11}C- or ^{3}H-methionine and particularly ^{3}H-thymidine accumulate to a lesser extent in infectious foci, although L-^{11}C- or ^{3}H-methionine has a reasonably high infection/blood uptake ratio. Since ^{18}F-FDG shows much higher infection/blood uptake ratios at early time points than does ^{67}Ga-citrate, ^{18}F-FDG-PET may prove useful in the rapid detection and monitoring of infections in man, and more detailed clinical study is warranted.

Acknowledgements. The authors thank the PET chemistry staff for their contributions. This work was supported by National Cancer Institute grants CA52880, CA53172 and CA56731.

References

1. Warburg O. *The metabolism of tumors*. New York, NY: Richard R. Smith; 1931: 129–169.
2. Johnstone RM, Scholefield PG. Amino acid transport in tumor cells. *Adv Cancer Res* 1965; 9: 143–226.
3. Lea MA, Morris HP, Weber G. Comparative biochemistry of hepatomas. VI. Thymidine incorporation into DNA as a measure of hepatoma growth rate. *Cancer Res* 1966; 26: 465–469.
4. Som P, Atkins HL, Bandoypadhyay D, et al. A fluorinated glucose analog, 2-fluoro-2-deoxy-D-glucose (F-18): nontoxic tracer for rapid tumor detection. *J Nucl Med* 1980; 21: 670–675.
5. Kubota K, Matsuzawa T, Ito M, et al. Lung tumor imaging by positron emission tomography using C-11 L-methionine. *J Nucl Med* 1985; 26: 37–42.
6. Wahl RL. Positron emission tomography: application in oncology. In: Murray IPC, Ell PJ, Strauss HW, eds. *Nuclear medicine in clinical diagnosis and treatment*. London: Churchill Livingstone; 1994: 801–820.
7. d'Argy R, Paul R, Frankenberg L, et al. Comparative double-tracer whole-body autoradiography: uptake of ^{11}C-, ^{18}F- and ^{3}H-labeled compounds in rat tumors. *Int J Rad Appl Instrum* [*B*] 1988; 15: 577–585.
8. Ishiwata K, Vaalburg W, Elsinga PH, Paans AM, Woldring MG. Comparison of L-[1-^{11}C]methionine and L-methyl-[^{11}C]methionine for measuring in vivo protein synthesis rates with PET. *J Nucl Med* 1988; 29: 1419–1427.
9. Larson SM, Weiden PL, Grunbaum Z, et al. Positron imaging feasibility studies. I: Characteristics of [^{3}H]thymidine uptake in rodent and canine neoplasms: concise communication. *J Nucl Med* 1981; 22:869–874.
10. Tahara T, Ichiya Y, Kuwabara Y, et al. High [^{18}F]-fluorodeoxyglucose uptake in abdominal abscesses: a PET study. *J Comput Assist Tomogr* 1989; 13: 829–831.
11. Sasaki M, Ichiya Y, Kuwabara Y, et al. Ringlike uptake of [^{18}F]FDG in brain abscess: a PET study. *J Comput Assist Tomogr* 1990; 14: 486–487.
12. Gutowski TD, Fisher SJ, Moon S, Wahl RL. Experimental studies of ^{18}F-2-fluoro-2-deoxy-D-glucose (FDG) in infection and in reactive lymph nodes [abstract]. *J Nucl Med* 1992; 33: 925.
13. Wahl RL, Fisher SJ. A comparison of FDG, L-methionine and thymidine accumulation into experimental infections and reactive lymph nodes [abstract]. *J Nucl Med* 1993; 34: 104p.
14. Lewis PJ, Salama A. Uptake of fluorine-18-fluorodeoxyglucose in sarcoidosis. *J Nucl Med* 1994; 35: 1647–1649.
15. Ichiya Y, Kuwabara Y, Sasaki M, et al. FDG-PET in infectious lesions: the detection and assessment of lesion activity. *Ann Nucl Med* 1996; 10: 185–191.
16. Alazraki NP. Gallium-67 imaging in infection. In: Early PJ, Sodee DB, eds. *Principles and practice of nuclear medicine*, 2nd edn. St. Louis: Mosby-Year Book; 1995: 702–713.
17. Alavi A, Buchpiguel CA, Loessner A. Is there a role for FDG PET imaging in the management of patients with sarcoidosis? [editorial]. *J Nucl Med* 1994; 35:1650–1652.
18. Larson SM. Cancer or inflammation? A Holy Grail for nuclear medicine [editorial]. *J Nucl Med* 1994; 35: 1653–1655.
19. Sugawara Y, Braun DK, Kison PV, Russo JE, Zasadny KR, Wahl RL. Rapid detection of human infections with fluorine-18 fluorodeoxyglucose and positron emission tomography: preliminary results. *Eur J Nucl Med* 1998; 25: 1238–1243.
20. McFarland J. The nephelometer: an instrument for estimating the number of bacteria in suspensions used for calculating the opsonic index and for vaccines. *JAMA* 1907; 49: 1176–1178.
21. Hendrickson DA, Krenz MM. Reagents and stains. In: Balows A, Hausler WJ, Herrmann KL, Isenberg HD, Shadomy HJ, eds. *Manual of clinical microbiology, 5th edn.* Washington, D.C.: American Society for Microbiology; 1991: 1296.
22. Eisenstein BI. Infectious diseases and their etiologic agents. In: Mandell GL, Bennett JE, Dolin R, eds. *Mandell, Douglas and Bennett's principles and practice of infectious diseases. 4th edn*. New York: Churchill Livingstone; 1995: 1964–1980.
23. Toorongian SA, Mulholland GK, Jewett DM, Bachelor MA, Kilbourn MR. Routine production of 2-deoxy-2-[^{18}F]fluoro-D-glucose by direct nucleophilic exchange on a quaternary 4-aminopyridinium resin. *Int J Rad Appl Instrum* [*B*] 1990; 17: 273–279.
24. Comar D, Cartron J, Maziere M, Marazano C. Labelling and metabolism of methionine-methyl-^{11}C. *Eur J Nucl Med* 1976; 1: 11–14.
25. Fraker PJ, Speck JC Jr. Protein and cell membrane iodinations with a sparingly soluble chloroamide, 1,3,4,6-tetrachloro-3a,6a-diphenylglycoluril. *Biochem Biophys Res Commun* 1978; 80: 849–857.
26. Kubota K, Ishiwata K, Kubota R, et al. Tracer feasibility for monitoring tumor radiotherapy: a quadruple tracer study with fluorine-18-fluorodeoxyglucose or fluorine-18- fluorodeoxyuridine, L-[methyl-^{14}C]methionine, [6-^{3}H]thymidine, and gallium-67. *J Nucl Med* 1991; 32: 2118–2123.
27. Wahl RL, Hutchins GD, Buchsbaum DJ, Liebert M, Grossman HB, Fisher S. 18F-2-deoxy-2-fluoro-D-glucose uptake into human tumor xenografts. Feasibility studies for cancer imaging with positron-emission tomography. *Cancer* 1991; 67: 1544–1550.
28. Pan HS, Frey KA, Young AB, Penney JB, Jr. Changes in [^{3}H]muscimol binding in substantia nigra, entopeduncular nucleus, globus pallidus, and thalamus after striatal lesions as demonstrated by quantitative receptor autoradiography. *J Neurosci* 1983; 3: 1189–1198.
29. Brown RS, Leung JY, Fisher SJ, Frey KA, Ethier SP, Wahl RL. Intratumoral distribution of tritiated fluorodeoxyglucose

in breast carcinoma: I. Are inflammatory cells important? *J Nucl Med* 1995; 36: 1854–1861.
30. Hoffer P. Gallium: mechanisms. *J Nucl Med* 1980; 21: 282–285.
31. Fantone JC, Ward PA. Role of oxygen-derived free radicals and metabolites in leukocyte-dependent inflammatory reactions. *Am J Pathol* 1982; 107: 395–418.
32. Osman S, Danpure HJ. The use of 2-[^{18}F]fluoro-2-deoxy-D-glucose as a potential in vitro agent for labelling human granulocytes for clinical studies by positron emission tomography. *Int J Rad Appl Instrum* [*B*] 1992; 19: 183–190.
33. Kubota R, Yamada S, Kubota K, Ishiwata K, Tamahashi N, Ido T. Intratumoral distribution of fluorine-18-fluorodeoxyglucose in vivo: high accumulation in macrophages and granulation tissues studied by microautoradiography. *J Nucl Med* 1992; 33: 1972–1980.
34. Yamada S, Kubota K, Kubota R, Ido T, Tamahashi N. High accumulation of fluorine-18-fluorodeoxyglucose in turpentine-induced inflammatory tissue. *J Nucl Med* 1995; 36: 1301–1306.
35. Weisdorf DJ, Craddock PR, Jacob HS. Glycogenolysis versus glucose transport in human granulocytes: differential activation in phagocytosis and chemotaxis. *Blood* 1982; 60: 888–893.
36. Minn H, Paul R, Ahonen A. Evaluation of treatment response to radiotherapy in head and neck cancer with fluorine-18 fluorodeoxyglucose. *J Nucl Med* 1988; 29: 1521–1525.
37. Cotran RS, Kumar V, Robbins SL. *Robbins pathologic basis of disease, 5th edn.* Philadelphia: W.B. Saunders; 1994: 51–92.
38. Bohnsack JF, Brown EJ. The role of the spleen in resistance to infection. *Ann Rev Med* 1986; 37: 49–59.
39. Anderson RL, Wood WA. Carbohydrate metabolism in microorganisms. *Ann Rev Microbiol* 1969; 23: 539–578.
40. Kubota K, Matsuzawa T, Fujiwara T, et al. Comparative study of tumor diagnosis using ^{11}C- and ^{13}N-labeled amino acids. *Kaku Igaku* 1985; 22: 981–987.
41. Tsukamura S, Mizuno S, Tsukamura M. Methionine metabolism of mice with mycobacterial infection and effect of prednisolone on it. *Jpn J Tuberc* 1966; 13: 43–48.
42. Hasselgren PO, Pedersen P, Sax HC, Warner BW, Fischer JE. Current concepts of protein turnover and amino acid transport in liver and skeletal muscle during sepsis. *Arch Surg* 1988; 123: 992–999.
43. von Allmen D, Hasselgren PO, Higashiguchi T, Frederick J, Zamir O, Fischer JE. Increased intestinal protein synthesis during sepsis and following the administration of tumour necrosis factor α or interleukin-1α. *Biochem J* 1992; 286: 585–589.
44. Rafferty JF, Noguchi Y, Fischer JE, Hasselgren PO. Sepsis in rats stimulates cellular proliferation in the mucosa of the small intestine. *Gastroenterology* 1994; 107: 121–127.
45. Kubota K, Matsuzawa T, Fujiwara T, et al. Differential diagnosis of AH109A tumor and inflammation by radioscintigraphy with L-[methyl-^{11}C]methionine. *Jpn J Cancer Res* 1989; 80: 778–782.